ingegneria sismica
International Journal of Earthquake Engineering
Anno XLIII - Num. 1 - 2026

Damage Mechanism and Deformation Optimization Design of Split-Connection Expansion Joints for Assembled Bridges Based on Damage Mechanics

Yujuan Liu[1] *and Chuan'ai Zhang*[1,*]

[1] Intelligent Construction College, Zhengzhou Business University, Zhengzhou, Henan, 451200, China

SUMMARY: *Due to the setting of expansion joints, it will increase the impact force when the vehicle passes through, leading to the structural damage or pavement damage of the assembled bridges at the joints, which is a relatively common phenomenon in many bridge structures. In this paper, starting from the ontological relationship under damage mechanics, combined with the theory of continuous medium thermodynamics, we explore the damage evolution equations in a general sense. Then, based on ANSYS finite element software, the elastic-plastic damage model and the intrinsic model of the expansion joints of assembled bridges are established, and the meshing and boundary conditions are set. The finite element simulation results show that when the load is applied to 1179.71KN, the reinforcement at the tap expansion joints starts to yield, and at this time, the sectional bending moment is 959.67KN·m, and there are differences in bearing capacity and deflection of assembled bridges with different materials. Under the standard axle load of 120kN, the maximum principal compressive stress of the material does not exceed 4.5MPa. In order to better enhance the performance of the assembled bridge tap expansion joints, an external T-beam can be used to enhance its stress bearing capacity and prevent deformation.*

KEYWORDS: *damage mechanics; damage evolution equation; ANSYS; assembled bridge expansion joints*

1 Introduction

Bridge expansion joints are becoming more numerous as the proportion of bridges in highways continues to rise. Although an expansion joint is only an auxiliary component of a bridge structure, it is located in the local discontinuous zone of the bridge deck system and is therefore regarded as a vulnerable part [1]. With the continued growth of traffic volume, vehicle load level, speeding, overloading, and repeated violations of traffic regulations, modern society has placed increasingly strict demands on driving safety and smooth traffic operation. As a result, higher requirements have been raised for the quality, durability, safety, and long-term stability of expansion joints and their anchorage zones [2-4].Since the expansion joint together with its anchorage area is usually the final item completed in bridge construction, it often receives insufficient attention during design, construction, maintenance, repair, and management. Consequently, it easily becomes a weak link, and subsequent repair or replacement frequently causes additional economic losses and broader social effects. Bridge expansion joints are often placed between the upper structure of two adjacent spans or between the beam and the back of

*liu942846@126.com
https://doi.org/10.65102/is2026197 Published: 30 April, 2026

the platform, mainly under the action of vehicle load, ambient temperature increase or decrease, concrete contraction, creep, can be free to expand and contraction deformation, but not a large deformation or jamming, to ensure that the vehicle is normal and smooth driving [5-7]. That is, try to ensure that under the load, environmental changes, expansion joint device can meet the bridge structure deformation caused by a variety of displacements, but also can effectively transfer the load to the beam.

As compared to other components of bridges, expansion joints in bridges are prone to structural damage because they are directly subjected to repeated impacts and crushing effects caused by traffic loads [8]. While the upfront cost associated with the construction of bridge expansion joints is relatively lower, the shorter lifespan will require more maintenance and replacement works, causing expenses for the maintenance and renewal of bridge expansion joints to reach up to one billion RMB annually. At the same time, repairs or replacements for bridge expansion joints usually involve traffic interruptions, especially those constructed on high-quality highways that are subject to higher traffic volumes and faster speed. In addition, damage or destruction of bridge expansion joints will increase the impact force exerted on the bridge deck, affecting its usual performance behavior and reducing its total lifespan [9, 10]. Moreover, damages or defects in bridge expansion joints may cause vehicles to jump when passing through movement inconsistencies, which could lead to a sudden feeling of fear among motorists and cause them to make irrational decisions, putting their safety at risk [11, 12]. Therefore, the consideration of the operating behaviors of bridge expansion joints in real-life applications along with their fatigue damage and deformation optimization analysis provides not only theoretical basis but also practical guidance for future maintenance efforts.

Because bridge expansion joints are closely associated with the overall structural safety of bridges, scholars have carried out extensive studies on both their global and local performance. Di Mascio et al [13] performed an exhaustive case study of a bridge expansion joint using 3D characterization, acceleration testing, and finite element modeling. This study brings out the significant role played by bridge expansion joints in enhancing driver safety and maintaining road surface smoothness, as well as offering information that can be used in developing more rational pavement designs. Abdel Raheem et al [14] assessed the effects of expansion joints on the seismic resistance capability of bridges. According to the researchers, changes in vibration characteristics caused by bridge construction may result in displacements, which become increasingly problematic after crossing a particular threshold and eventually affect seismic performance. On this basis, they came up with a list of guidelines for reducing seismic risks, which are suitable for both old and new bridges. Cho et al [15] pointed out that rubber-joint expansion joints can experience damage from various sources. For this reason, they sought to create a new expansion joint design, made of superelastic shape-memory alloy, whose efficiency was confirmed via finite-element analysis. The outcome of this research holds great promise for improving the durability and safety of bridge facilities. Li, J et al [16] analyzed the effects of damaged bridge expansion joints on the natural frequencies of concrete beams, struts, and anchorage regions. In their experiment, they identified six different damage conditions in three samples. The test results showed that bridge expansion joints are continuously exposed to environmental conditions and hence vulnerable to damage resulting from traffic loads repeatedly applied on them, an observation consistent with previous research findings. Friedl et al [17] based on the classical frequency method of complex transfer matrix completely describes the dynamic behavior of the vehicle as well as the spectral density matrix characterizing the roughness of the road surface, establishes a three-dimensional finite element expansion joint model with non-proportional damping, and analyzes the amplification of the dynamic response of the expansion joints, and the results show that the dynamic response characteristics of the bridge expansion joints are mainly determined by the discrete spring elements.

Research in the same period also showed that damage to bridge expansion joints mainly appears in the form of fatigue failure. For example, Stamatopoulos [18] focused on fatigue failure of anchor bolts at the connection between the supporting crossbeam and the center girder. By establishing a three-dimensional finite-element model for a single-support beam modular expansion joint and applying nodal fatigue loading to the bolted connection, that study showed that even after 10 million fatigue-loading cycles, expansion joints do not necessarily exhibit sufficient fatigue life at the structural details. Therefore, evaluation of joint fatigue life should be combined with the nodal fatigue-load model in order to more fully reflect actual fatigue behavior. Chang et al [19] through research on different expansion-joint types and corresponding repair issues, found that early failure of the anchorage zone is mainly caused by insufficient strength and toughness. Under dramatic growth in traffic flow and heavy vehicles, premature traffic opening further aggravated concrete deterioration, which then caused early anchorage-zone failure and eventually led to destruction of the expansion device. Guo et al [20] investigated the damage mechanism of control springs in bridge expansion joints. By measuring the relative motion of plate layers at different locations, they found that movement of the plate layers near the joints was much more intense, thereby causing more serious spring damage. Static and dynamic finite-element analyses provided strong support for this conclusion. Sun, Z et al [21] designed three test scenarios for studying bridge-joint damage mechanisms, including a static test, an impact line test, and a truck-passing test. Their results showed that expansion-joint damage was affected by bridge deformation in the static and impact-line tests, whereas the truck test indicated that vehicle-axle load was another important cause. Ma et al [22] carried out static-load and fatigue tests on a shallow-buried modular expansion joint and found that increasing fatigue load amplitude reduced overall joint stiffness. Under standard axial loading, fatigue life was 1.9 times that under overload conditions, and overloading exerted a stronger influence on both stiffness and fatigue life. Ji et al [23] identified the fatigue factor of the critical structure near expansion joints in corrugated-steel-web combined steel box-girder bridges on the basis of a vehicle－bridge coupled vibration system. Their findings showed that stress impact coefficient and stress-amplitude impact coefficient are the key indicators leading to joint damage, while the spacing between the critical structure and the expansion joint plays a decisive role in the interaction between the two. Sun, Z et al [24] also conducted a fatigue-life assessment of bridge expansion joints through traffic-load modeling, numerical analysis of expansion-joint loads, and fatigue-life evaluation. This method successfully revealed damage effects caused by loss of sliding springs on center beams, while also examining the effects of traffic speed, horizontal impact components, surface irregularities, and damping ratios on expansion joints. Coelho et al [25] further conducted different types of fatigue-related studies in this field. They conducted different types of fatigue loading experiments on expansion joint structures subjected to fatigue loading at the expansion joints of the Martinus Nijhoff Bridge in the Netherlands. Strain measurements were taken for a number of different working conditions of the beam fixing device when different vehicle speeds were passing through, which were verified by numerical simulations, and the effects of the beam fixing device on the expansion joints and the vehicle speed on the strain center distribution of the center beam were derived.

With the continuous development of the related fields, there have been many studies on health monitoring of bridge expansion joints and improvement of corresponding detection approaches, modalities, accuracy, and efficiency. Li, J et al [26] established a damage assessment framework of bridge expansion joints in order to identify damage to concrete in the center girder, support rods, and anchoring areas. By means of numerical simulation, the identification accuracy was found to be high for different kinds of damage to bridge expansion joints. Chen et al [27] made use of long-term monitoring data to conduct damage detection of bridge expansion joints. With the help of principal component analysis (PCA), the key data features were extracted, followed by developing a temperature-displacement relationship using least squares support vector machine in order to reduce the effect of temperature variables on each other. After parameter optimization, the Pauta criterion was introduced to determine the damage threshold of bridge expansion joints and achieve successful damage detection. Ni et al [28] established a condition assessment and early warning model for bridge expansion joints from a Bayesian viewpoint to avoid the potential social hazards due to failure of bridge expansion joints. The probabilistic approach was able to monitor data uncertainty and quantify model error, making it suitable for long-term health monitoring of bridge expansion joints. Dong et al [29] improved the traditional traffic load simulation technique with transformer technology and applied it in the monitoring of wear resistance in bridge expansion joints, demonstrating superiority of their method compared to the traditional comparative data-driven approaches in terms of $R^2 = 0.96619$. On the contrary, Ni et al [30] proposed an assessment approach to evaluate the safety level of bridges based on long-term monitoring data and reliability analysis, setting up safety evaluation criteria for managers of bridge.

To further improve the optimization of damage mechanisms and deformation design for assembled bridge-deck expansion joints, this study analyzes the mechanical behavior of assembled bridge-tap expansion joints using damage mechanics and finite-element models. The results provide a new way to optimize parameter settings for assembled bridge-tap expansion joints, enhance their structural stability, and help prevent possible safety accidents caused by damage to expansion joints.

2 Ontological relationships and evolutionary equations for damage mechanics

Expansion joints are an important component of assembled bridge structures and also one of their weak parts. Under the repeated action of wheel pressure, they are vulnerable to strength deterioration and fatigue damage, and the resulting maintenance expenditure for expansion joints may account for up to 20% of the total bridge maintenance cost. Therefore, the strength and fatigue problems of expansion joints have become an important issue in current assembled-bridge engineering.

2.1 Ontological Relationships in the Damage State

2.1.1 Damage variables and related parameters

A researcher, who considers the extension of defects as the main cause of material damage, defines the continuity variable as:

$$\psi = \frac{\tilde{A}}{A} \tag{1}$$

where $\tilde{A}$ is the actual bearing area, i.e., the area obtained after deducting the portion that cannot bear due to defects, and A is the nominal area, i.e., the initial area.

Due to the existence of micro-cracks and micro-holes, the effective bearing area decreases and the net stress per unit area increases. Let σ be the stress when there is no microcrack or hole, i.e. Cauchy stress, and the stress acting on the specimen in uniaxial tension is:

$$P = \sigma \times A = \tilde{\sigma} \times \tilde{A} \tag{2}$$

where $\tilde{\sigma}$ is the net or effective stress. From equation (2) and equation (1):

$$\tilde{\sigma} = \frac{\sigma}{\psi} \tag{3}$$

and introduces the concept of impairment variables, i.e:

$$D = 1 - \psi = 1 - \frac{\tilde{A}}{A} \tag{4}$$

$A - \tilde{A}$ is the area that cannot be carried after damage, so the net stress can be expressed as:

$$\tilde{\sigma} = \frac{\sigma}{1 - D} \tag{5}$$

The value of D should be between 1 and 0. When $D = 0$, it corresponds to the case of no damage, and when $D - 1$, it means that the material is completely destroyed.

The analysis of equivalent stresses is based on the method of continuum mechanics. That is, the material under consideration should be continuous and homogeneous. The stress for uniaxial loading can be expressed as:

$$\sigma = P / A \tag{6}$$

In research, VonMises equivalent force is needed, which has been widely used in plastic mechanics. The equivalent force σ_e can be expressed as:

$$\sigma_e = \sqrt{\frac{3}{2} S_{ij} S_{ij}}\ (i, j = 1, 2, 3) \tag{7}$$

where S_{ij} -variation of the stress bias component, which is equal to:

$$S_{ij} = \sigma_{ij} - \frac{1}{3} \delta_{ij} \delta_{rs} \sigma_{rs} \tag{8}$$

Format:

$$\delta_{ij} = \begin{cases} 1, (i = j) \\ 0, (i \neq j) \end{cases} \tag{9}$$

In order to formulate the stress-strain relationship for a material, some assumptions need to be made as follows:

(1) The member material should be considered elastic and have a maximum stress below the yield limit of its material.

(2) The material is homogeneous, that is, the points in the member have the same properties before loading.

(3) The damage to the material is isotropic before loading.

2.1.2 Ontological Relationships in the Damage State

The description of the intrinsic relationship under the damage state is an important content to describe the material fatigue damage, which reflects the bearing capacity and mechanical properties of the damaged material, and is crucial for constructing the fatigue damage evolution relationship and describing the fatigue damage process. According to the actual specific loading form, material properties, damage type and other factors to determine the basic form of the damage variable, often to carry out the calculation of the effective bearing area, which is very difficult for random damage type and damage process. Strain equivalence hypothesis is more ideal to realize the indirect measurement of damage, the core idea of this assumption is: whether the material produces damage or not, in the same equivalent force, the effective bearing plane of the micrometabolite body to produce the same amount of strain. In other words, the deformation behavior of the damaged material can be obtained from the intrinsic relationship of the undamaged material. According to Eq. (7), when the material obeys the elastic ontological relationship, there is:

$$\sigma_E = E\varepsilon \tag{10}$$

To wit:

$$\sigma = \begin{cases} (1-D)E\varepsilon & (\sigma \geq 0) \\ (1-hD)E\varepsilon & (\sigma < 0) \end{cases} \tag{11}$$

According to the above equation, the modulus of elasticity in the tensile and compressive damage states can be defined as $E_{E,I}, E_{E,C}$, respectively, then it has the following form:

$$\begin{aligned} E_{E,T} &= (1-D)E(\sigma \geq 0) \\ E_{E,C} &= (1-hD)E(\sigma < 0) \end{aligned} \tag{12}$$

Assuming that the instantaneous damage can be determined by the tensile modulus, $D = 1 - \frac{E_{E,T}}{E}$, then the value of the parameter h can be calculated by the following equation:

$$h = \frac{E - E_{E,C}}{E - E_{E,T}} \tag{13}$$

2.2 Damage evolution equations in a general sense

2.2.1 Fundamentals of continuum mechanics

The first law of thermodynamics refers to the principle of energy conservation. It states that the variation in the internal and kinetic energy of a thermodynamic system within a unit time interval equals the total work performed on the system during that interval by internal and external forces, together with the energy transferred between the system and the surrounding environment. The corresponding energy equation can be written as follows:

$$\rho\dot{e} = \sigma_{ij}\dot{\varepsilon}_{ij} + \rho\dot{\gamma} - \dot{q}_{i,i} \tag{14}$$

where ρ is the medium mass density, e is the internal energy per unit mass of medium, ε_{ij} is the strain tensor, σ_{ij} is the stress tensor conjugate to the work of ε_{ij}, γ is the heat released by unit mass of medium, and $q_{i,i}$ is the heat flux. "·" is the material derivative of a physical quantity, which represents the rate of change of the corresponding physical quantity per unit time.

The damage process of a material is essentially an irreversible process of energy dissipation, assuming that the dissipation potential is described from the plastic deformation part φ_p and the damage part φ_D as:

$$\varphi = \varphi_p\left(\sigma, \sigma_Y, R, D\right) + \varphi_D\left(Y, p, T, \varepsilon^e, D\right) \tag{15}$$

where σ_Y is the initial yield stress of the material and R is the hardening parameter for isotropic cumulative plastic strain.

For linearly elastic and isotropic materials, the damage equation is expressed as follows:

$$\sigma_{ij} = \rho \frac{\partial g}{\partial \varepsilon_{ij}^e} = \alpha_{ijkl}\varepsilon_{kl}^e(1-D) \tag{16}$$

$$\varepsilon_{ij}^e = \frac{1+v}{E}\frac{\sigma_{ij}}{1-D} - \frac{v}{E}\frac{\sigma_{kk}}{1-D}\delta_{ij} \tag{17}$$

$$Y = -\frac{\sigma_{eq}^2}{2E(1-D)^2}R_v \tag{18}$$

where R_v is the triaxial function for:

$$R_v = \frac{2}{3}(1+v) + 3(1-2v)\left(\frac{\sigma_H}{\sigma_{eq}}\right)^2 \tag{19}$$

where α_{ijkl} is the elasticity tensor, v is the Poisson's ratio, δ_{ij} is the Kronecker notation, σ_{eq} is the VonMises equivalent stress, σ_H is the hydrostatic pressure, σ_{ij}^D is the stress deflection tensor.

Where:

$$\delta_{ij} = \begin{cases} 0, & i \neq j \\ 1, & i = j \end{cases} \tag{20}$$

$$\sigma_{eq} = \left(\frac{3}{2}\sigma_{ij}^D\sigma_{ij}^D\right)^{\frac{1}{2}} \tag{21}$$

$$\sigma_{ij}^D = \sigma_{ij} - \delta_{ij}\sigma_H \tag{22}$$

$$\sigma_H = \frac{1}{3}\sigma_{kk} \tag{23}$$

The dissipative part of the corresponding plasticity is:

$$\varphi_p = \frac{\left(\sigma_{eq} - R\right)}{(1-D)} - \sigma_Y \tag{24}$$

Decomposing the strain rate and introducing a constant positive scalar multiplier λ yields a plastic strain rate of:

$$\dot{\varepsilon}_{ij}^p = \dot{\lambda}\frac{\partial \varphi_p}{\partial \sigma_{ij}} = \frac{3}{2}\frac{\dot{\lambda}}{1-D}\frac{\sigma_{ij}^p}{\sigma_{eq}} \tag{25}$$

The cumulative plastic strain rate is:

$$\dot{p} = -\dot{\lambda}\frac{\partial \varphi_p}{\partial R} = \frac{\dot{\lambda}}{1-D}\left[\frac{2}{3}\dot{\varepsilon}_{ij}^p\dot{\varepsilon}_{ij}^p\right]^{\frac{1}{2}} \tag{26}$$

2.2.2 Damage evolution equations

The elastic modulus of a material gradually declines as damage develops. It is generally assumed that damage is associated with the elastic behavior of the material, so the elastic component of free energy is linked to the damage variable, whereas the plastic hardening work term does not represent damage. This assumption is commonly regarded as consistent with the damage driving force defined in damage mechanics. Accordingly:

$$g^{(T)} = \Gamma_e\left(\varepsilon_{ij}^e, T, D\right) + \Gamma_p\left(\alpha_{ij}, T, P\right) \tag{27}$$

where $g^{(T)}$ is the actual free energy function, Γ_p is the plastic hardening work function, α_{ij} is the back stress tensor, and P is the cumulative plastic strain, which has the value $P = \sqrt{\left(2/3\varepsilon_{ij}^p : \varepsilon_{ij}^p\right)}$. When the fatigue damage is assumed to be an isothermal process, the elastic part of the Helmholtz free energy coupled to the damage variable can be expressed as:

$$\Gamma_e = \frac{1}{2\rho}S_{ijkl}\varepsilon_{kl}^e\varepsilon_{ij}^e(1-D) \tag{28}$$

Then the damage driver is expressed in the form:

$$-Y = \frac{1}{2}S_{ijkl}\varepsilon_{kl}^e\varepsilon_{ij}^e \tag{29}$$

From the theory of elastic mechanics it can be derived that under isotropic damage conditions equation (29) expands in the form of:

$$-Y=\frac{\sigma_{\mathrm{eq}}^{2}}{2E(1-D)^{2}}\left[\frac{2}{3}(1+v)+3(1-2v)\left(\frac{\sigma_{\mathrm{H}}}{\sigma_{\mathrm{eq}}}\right)^{2}\right] \tag{30}$$

where σ_{eq} is the VonMises equivalent force with the value $\sigma_{\mathrm{eq}}=\sqrt{\left(3/2\sigma_{ij}:\sigma_{ij}\right)}$. In addition, $R_{\mathrm{v}}=2(1+v)/3+3(1-2v)\left(\sigma_{\mathrm{H}}/\sigma_{\mathrm{eq}}\right)^{2}$ can be reduced and merged, and R_{v} is defined in the damage mechanics as the triaxial factor.

Both the plastic strain process and the damage evolution process are irreversible dissipative work processes. For the damage process, it should be satisfied:

$$-YD>0 \tag{31}$$

By the non-negativity of the damage driver and the form of the expression, there is necessarily:

$$\dot{D}>0 \tag{32}$$

This equation shows that the damage value is increasing by thermodynamic self-consistency.

Suppose there exists a certain dissipative potential function Ω as a function of all generalized strains, i.e., $\Omega\left(\dot{\varepsilon}_{ij}^{p},\dot{P},\dot{D},\dot{q}_{i}\right)$, or after the Legendre transformation yields the expression $\Omega^{*}\left(\sigma_{ij},R,-Y,-T_{i}/T\right)$ with respect to the dyadic generalized force, and according to the orthogonal flow law the expression of the dyadic generalized force dissipation potential function for the damage evolution equations can be obtained as:

$$\dot{D}=\frac{\partial\Omega^{*}}{\partial(-Y)} \tag{33}$$

When constructing the potential function for damage dissipation, the expression of the damage-evolution equation is established according to the assumption of strain equivalence and experimental observations. Under the condition that both plasticity and damage are isotropic, the damage-dissipation potential function may be written as:

$$\Omega^{*}=\frac{S_{1}}{S_{0}+1}\left(\frac{-Y}{S_{1}}\right)^{S_{0}+1}\dot{P} \tag{34}$$

where S_{0},S_{1} are temperature-dependent material parameters. From this, a damage evolution equation of the type t in the general sense can be obtained based on Eq. (33) described as:

$$\dot{D}=\left(\frac{-Y}{S_{1}}\right)^{S_{0}}\dot{P} \tag{35}$$

The continuous evolution of fatigue damage is ultimately due to the continuous accumulation of plastic strain.

3 Finite element modeling of assembled bridge expansion joints

The primary function of assembled bridge expansion joints is to accommodate the free deformation of the girder and bridge deck. At the same time, they also serve to reinforce the girder end and fill the gap between adjacent girders, making them an important auxiliary component in bridge engineering. The quality and durability of assembled bridge expansion joints directly influence traffic safety, vehicle comfort, and driving speed, and they also affect the service life of the joints themselves.

3.1 Elastic-plastic damage model for expansion joints

3.1.1 Plastic and damage models

The plasticity model includes a yield criterion, a flow rule, a hardening law, and a hardening function. In damaged materials, internal forces are borne by the effective part of the material. Therefore, it is reasonable to assume that plastic deformation takes place in the undamaged region of the damaged material. The equivalent plastic strain $\tilde{\varepsilon}_{\mathrm{p}}$, and the effective stress $\bar{\sigma}$ are formulated on the basis of the effective-stress space. The plastic yield criterion can be written as follows:

$$F\left(\bar{\boldsymbol{\sigma}},\tilde{\boldsymbol{\varepsilon}}_p\right)=F_p(\bar{\boldsymbol{\sigma}})-\kappa\left(\tilde{\boldsymbol{\varepsilon}}_p\right)=0 \tag{36}$$

where is F_p is the plastic potential function and κ is the reinforcement function, which is used to express the relationship between yield variables and plastic deformation, so as to determine the extension law of the yield surface.

The yield criterion is adopted as Drucker-Prager plastic yield criterion, i.e.:

$$F\left(\bar{\boldsymbol{\sigma}},\tilde{\boldsymbol{\varepsilon}}_p\right)=\alpha I_1+\sqrt{J_2}-\kappa\left(\tilde{\boldsymbol{\varepsilon}}_p\right)=0 \tag{37}$$

where is α is the internal friction of the material and I_1 and J_2 are the stress invariants.

Considering that $\boldsymbol{\kappa}$ is related to the degree of total plastic deformation, an equivalent plastic strain increment is introduced, viz:

$$\mathrm{d}\boldsymbol{\varepsilon}_{\mathrm{p}}=\sqrt{\frac{2}{3}\left[\left(\mathrm{d}\tilde{\boldsymbol{\varepsilon}}_{i,j}\right)_p\left(\mathrm{d}\boldsymbol{\varepsilon}_{i,j}\right)_p\right]} \tag{38}$$

Since the yield criterion is independent of hydrostatic pressure, i.e., the bioplastic strain increment is the same as the plastic strain increment, the strengthening parameter is:

$$\boldsymbol{\kappa}=\tilde{\boldsymbol{\varepsilon}}_p \tag{39}$$

Assuming that the equivalent plastic strain rate complies with the correlation flow law, the plastic strain rate is:

$$\left(\mathrm{d}\tilde{\boldsymbol{\varepsilon}}_{i,j}\right)_p=\mathrm{d}\lambda\frac{\partial f}{\partial\tilde{\sigma}_{i,j}} \tag{40}$$

where is $\mathrm{d}\lambda$ is the plasticity multiplier.

In order to distinguish the difference between the material's tensile and compressive damage evolution processes, a spectral decomposition of the stress is adopted, i.e:

$$\bar{\boldsymbol{\sigma}}^{+} = \sum_{i} \langle \bar{\boldsymbol{\sigma}}_{i} \rangle \mathbf{p}_{i}\mathbf{p}_{i}^{\mathrm{T}}, \bar{\boldsymbol{\sigma}} = \boldsymbol{\sigma} - \bar{\boldsymbol{\sigma}}^{+} \tag{41}$$

where $\langle \ \rangle$ is the MaCaulay bracket and $\mathbf{p}_i$ is the unit-column vector in the main direction of the effective force.

To consider the multiaxial stress state, the tensile shear stress $\left(\tau^{+}\right)$ and the compressive shear stress $\left(\bar{\tau}^{-}\right)$ are introduced as:

$$\bar{\tau}^{+} = \sqrt{\left(\bar{\boldsymbol{\sigma}}^{+}\right)^{\mathrm{T}} D\bar{\boldsymbol{\sigma}}^{+}}, \bar{\tau}^{-} = \sqrt{\sqrt{3}\left(K\bar{\sigma}_{8} + \bar{\tau}_{8}\right)} \tag{42}$$

The equation is $\bar{\sigma}_8$ for octahedral positive stress, $\bar{\tau}_8$ for octahedral shear stress, and $K = \sqrt{2} \times \dfrac{1-R_0}{1-2R_0}, R_0$ for the ratio of biaxial isobaric compressive strength of the masonry to uniaxial isobaric compressive strength.

According to the material material properties test, there exists an elastic phase without damage before the occurrence of tensile and compressive damage, therefore, it is necessary to define the threshold of initial damage to determine the material into a nonlinear state, the tensile damage threshold $\left(r_0^{+}\right)$ and the compressive damage threshold $\left(r_0^{-}\right)$ are:

$$r_0^{+} = \frac{f_{\mathrm{t}}}{\sqrt{E}}, r_0^{-} = \sqrt{\sqrt{\frac{2}{3}} \frac{R_0}{1-2R_0} f_0} \tag{43}$$

where f_0 and f_{t} are the initial yield strength and tensile strength under compression, respectively, and E is the elastic modulus of the material.

Then the damage evolution equation is:

$$d^{+} = 1 - \frac{r_0^{+}}{\bar{\tau}^{+}} e\left[A^{+}\left(1 - \frac{\bar{\tau}^{+}}{r_0^{+}}\right)\right], d^{-} = 1 - \frac{r_0^{-}}{\bar{\tau}^{-}}\left(1 - A^{-}\right) - A^{-} e^{\left[B^{-}\left(1 - \frac{\bar{\tau}^{-}}{r_0^{-}}\right)\right]} \tag{44}$$

where A^{-}, B^{-} are the model parameters of the compressive damage evolution equation, calibrated by the uniaxial compressive damage curve, and A^{+} is the model parameter of the tensile damage evolution equation, in order to avoid the mesh sensitivity of the calculation results, A^{+} is defined as:

$$A^{+} = \left(\frac{G_t E}{l_c f_t^2} - 0.5\right)^{-1} \geqslant 0 \tag{45}$$

where G_f is the tensile fracture energy, and l_c is the characteristic length of the crack, which takes the values $\sqrt[3]{V}, V$ as the solid unit volume.

3.1.2 Fatigue damage finite element modeling

In this study, an uncoupled anisotropic damage model is adopted. It is assumed that the principal axis of damage, the principal stress axis, and the principal strain axis coincide with one another, while the initial material state is taken as an isotropic elastomer. After damage occurs, the material exhibits orthogonal anisotropic properties. By comparing the stress-strain relationship of the orthogonally anisotropic undamaged material in the three-dimensional problem, the effective damage elasticity matrix in the three-dimensional principal coordinate system can be obtained, together with the stress-strain relation of the damaged material under that coordinate system. Specifically:

$$\left[\tilde{E}\right]=\begin{bmatrix} (\lambda+2\mu)(1-D1)^2 & \lambda(1-D1)(1-D2) & \lambda(1-D1)(1-D3) & 0 & 0 & 0 \\ \lambda(1-D1)(1-D2) & (\lambda+2\mu)(1-D2)^2 & \lambda(1-D2)(1-D3) & 0 & 0 & 0 \\ \lambda(1-D1)(1-D3) & \lambda(1-D2)(1-D3) & (\lambda+2\mu)(1-D3)^2 & 0 & 0 & 0 \\ 0 & 0 & 0 & \mu(1-D2)(1-D3) & 0 & 0 \\ 0 & 0 & 0 & 0 & \mu(1-D1)(1-D3) & 0 \\ 0 & 0 & 0 & 0 & 0 & \mu(1-D2)(1-D1) \end{bmatrix} \tag{46}$$

where is λ, μ is the Lame's constant, $\lambda=\dfrac{Ev}{(1+v)(1-2v)}, \mu=\dfrac{E}{2(1+v)}$, E, v are the modulus of elasticity and Poisson's ratio, respectively, and D_1, D_2, D_3 are the components of the equivalent damage in the three principal directions, respectively.

The matrix form of the effective damage elasticity tensor in the three-dimensional case is equivalent to the unit stiffness matrix specified in the principal coordinate system. Using the method of transformation of coordinates, the matrix form of the effective damage elasticity tensor in any coordinate system can be derived based on the principle coordinate form according to the following expression:

$$[E]=[T]^T[\tilde{E}][T] \tag{47}$$

which is $[E]=E_{ij},[\tilde{E}]=\tilde{E}_{ij},[T]=T_{ij}$.

In the current research work, the UMAT user material subroutine in ABAQUS is designed such that the effective damage elasticity matrix of the three-dimensional problem can be implemented into the fully coupled analysis of damage and stress-strain fields. In addition, in order to perform the finite element analysis of the damage phenomenon, the method of varying stiffness is utilized, wherein the unit stiffness matrix is updated at each step after every predetermined number of cycles of stresses in order to incorporate the effect of the fatigue damage on the unit stiffness matrix.

3.2 Finite element modeling of expansion joints

3.2.1 Main steps in finite element analysis

As a widely used finite element software, ANSYS can analyze structures, fluids, electromagnetic fields and coupled fields, which mainly includes three modules: pre-processing, analytical calculations and post-processing. The main steps of using finite element software ANSYS analysis are as follows:

(1) Establish a finite element model. First of all, according to the analysis of the actual problem and the purpose of the analysis, the model of the structure to do an appropriate simplification, and the establishment of the entity model, the establishment of the entity model there are two ways, one of which is to establish the model directly in the ANSYS software, the applicable object is the model of the structure of the relative simplicity. The second method is to establish the model to be studied through professional solid modeling software, and then imported into ANSYS software, applicable to the model structure is relatively complex. Then the unit type and material properties are defined, and finally the size of the unit and the calculation scale are determined according to the purpose of analysis, and the established solid model is meshed.

(2) Determine the boundary conditions of the structure. The establishment of load and boundary conditions is the most important and difficult work in the whole analysis process, first of all, we should establish the load and boundary conditions in line with the actual. Secondly, analyze the load and the characteristics of the structure to be studied, and consider whether the model can be simplified so that the structure reduces the amount of calculation and improves the efficiency of the calculation.

(3) Enter the analysis and calculation module, apply constraints and loads to the model, and solve.

(4) Enter the post-processing module to analyze and process the results obtained from the solution.

3.2.2 Expansion joint principal model design

Taking into consideration the fatigue damage finite element analysis model developed above, this study will make use of the ANSYS finite element program to conduct simulations on the component being studied. The initial pre-requisite for conducting finite element analysis involves establishing the inherent constitutive relationship of the material in question. In essence, the success of finite element analysis is dependent on the creation of the constitutive model of the material under investigation and the ability of experimental results from the material to fit into the model. This is essential in the formation of an appropriate finite element model. Constitutive relationship of a material refers to its stress strain relationship when subjected to external loads. In this study, the modular expansion joint used in assembled bridges is investigated. There are two basic materials involved namely; steel and concrete.

(1) Intrinsic relationship model of steel reinforcement

Shear nails, reinforcing bars and outer cladding steel plate are used in elastic-plastic hardened section, two-fold plasticity principal constitutive relationship model.

In the elastic phase, i.e., when $\varepsilon_s < \varepsilon_y$, the stress-strain relationship is known from elastic mechanics:

$$\sigma_s = E_s \varepsilon_s \tag{48}$$

At the stage of plastic strengthening, i.e., $\varepsilon_y \le \varepsilon_s \le \varepsilon_{s,u}$, the stress-strain relationship is given by the simplified relationship:

$$\sigma_s = f_y + \left(\varepsilon_s - \varepsilon_y\right) E_s' \tag{49}$$

where is σ_s is the magnitude of stress in the rebar, ε_s is the magnitude of strain in the rebar, ε_y is the magnitude of strain in yielding of the rebar, $\varepsilon_{s,u}$ is the magnitude of The magnitude of strain at reinforcement damage, E_s is the elastic modulus of the rebar, and E_s' is the modulus of the rebar in the plastic strengthening stage.

(2) Concrete principal relationship model

The concrete constitutive relationship is adopted in the concrete structure design code. Where the concrete uniaxial tensile $\sigma-\varepsilon$ curve is determined by the following equation:

$$\sigma=\left(1-d_{\mathrm{t}}\right)E_{\mathrm{c}}\varepsilon \tag{50}$$

$$d_t=\begin{cases}1-\rho_t\left[1.2-0.2x^5\right] & x\le 1\\ 1-\dfrac{\rho_t}{\alpha_t(x-1)^{1.7}+x} & x>1\end{cases} \tag{51}$$

$$x=\frac{\varepsilon}{\varepsilon_{t,r}} \tag{52}$$

$$\rho_t=\frac{f_{t,r}}{E_c\varepsilon_{t,r}} \tag{53}$$

where α_t is the value of the descending section of the uniaxial tensile $\sigma-\varepsilon$ curve, $f_{t,r}$ is the representative value of the uniaxial tensile strength of concrete, $\varepsilon_{t,r}$ is the value of peak tensile strain of concrete corresponding to the representative value of Concrete uniaxial tensile strength representative value $f_{t,r}$ corresponds to the peak tensile strain of concrete, d_t is the concrete uniaxial tensile damage evolution parameter.

The concrete uniaxial compression $\sigma-\varepsilon$ curve is determined by the following equation:

$$\sigma=\left(1-d_{\mathrm{c}}\right)E_{\mathrm{c}}\varepsilon \tag{54}$$

$$d_c=\begin{cases}1-\dfrac{\rho_c n}{n-1+x^n} & x\le 1\\ 1-\dfrac{\rho_c}{\alpha_c(x-1)^2+x} & x>1\end{cases} \tag{55}$$

$$\rho_c=\frac{f_{c,r}}{E_c\varepsilon_{c,r}} \tag{56}$$

$$n=\frac{E_c\varepsilon_{c,r}}{E_c\varepsilon_{c,r}-f_{c,r}} \tag{57}$$

$$x=\frac{\varepsilon}{\varepsilon_{c,r}} \tag{58}$$

where α_c is the value of the parameter of the descending section of the concrete uniaxial compression $\sigma-\varepsilon$ curve, $f_{c,r}$ is the representative value of the uniaxial compressive strength of the concrete, $\varepsilon_{c,r}$ is the peak tensile strain of the concrete corresponding to the representative value of the uniaxial compressive strength of the concrete $f_{c,r}$, d_c is the evolution parameter of the uniaxial compression damage of the concrete, and E_c is the modulus of elasticity of the concrete.

(3) Concrete plastic damage model

When analyzing the damage damage mechanism and deformation optimization of assembled bridge joint expansion joints, the moral plastic damage model involved is consistent with Section 3.1.2. In addition, other material parameters are defined, including the concrete expansion angle is taken as 360°, and the cohesion coefficient is taken as 0.005. The other three parameters are taken as default values according to the software help document, i.e., the flow potential offset is taken as 0.15, the ratio of the biaxial isobaric yield strength to the uniaxial compressive strength is taken as 1.15, and the ratio of the tensile meridian to the compressive meridian constant stress is taken as 0.665.

3.2.3 Mesh Division and Boundary Conditions

(1) Mesh selection, delineation and optimization. In the application of Damage Mechanics-Effective Stress Method, we note that damage prediction is sensitive to the coarseness of mesh division. This type of problem is mainly considered in the case of stress or strain, where a relatively fine mesh should be used for important parts and a slightly coarser mesh can be used for other parts. Therefore, mesh optimization is important for the specimen under study. In the numerical analysis study, the life of the studied member with initial damage degree and critical stress is investigated. According to the finite element experience about meshing, the finer the meshing, the more accurate the calculation results. ANSYS is used to mesh the model and refine the part where the stress is concentrated.

(2) Damage judgment criteria for units and components. In fact, for most of the materials, it is not the damage is 1 when the damage is destroyed, but before that, the damage reaches a certain value (known as the critical damage of the material), the material will be destroyed very quickly. The critical damage can be determined experimentally. Damage to the component can be judged according to the number of damaged units, that is, the same cross-section if a certain number of units destroyed that is, the component is considered completely destroyed.

4 Finite element simulation analysis of assembled bridge taps

As an important component of the bridge, the role of expansion joints is to make the bridge structure in the temperature change, concrete contraction, creep, and live load and other factors, can be free to expansion and contraction. Given that bridge expansion joints are constantly subjected to the effect of wheel loads, any surface irregularity caused by wheel loads will result in considerable impact damage to the deck of the bridge. Expansion joints that are continuously exposed to atmospheric conditions face rather harsh environments, thereby becoming one of the weakest parts of the entire bridge structure.

4.1 Damage mechanism of assembled bridge expansion joints

4.1.1 Load-displacement curves

The length of the finite element model used is 5.5 m, while the bearing distance and end girder distance used are 1.0 m and 0.15 m, respectively. For the support, there is a sliding bearing at one end of the left bearing where UY= 0, while for the right end, UX = 0, UY = 0, and UZ = 0, thus creating a fixed bearing. Transverse force is acted on the girder ends for a width of 0.5 m, while for the longitudinal forces, a width of 0.3 m acts from both sides on the girder ends, hence making a longitudinal force distance of 0.5 m. When assembling the bridge in use, the connection between the steel girder and concrete slab is mainly achieved using shear connections that are not modeled and have a bonded-contact interface.

The nonlinear analysis of concrete can capture the stress redistribution that occurs after cracking and can better simulate the mechanical response of both concrete and steel reinforcement. The nonlinear finite-element results for the bridge deck connection plate indicate that concrete cracking begins at 7.63×10^{-5}, so the bending moment corresponding to that strain is the cracking moment of the concrete, and the cracking moment of the bridge deck connection plate section is 112.53 kN·m. Once the tensile stress in concrete reaches the cracking strength, the concrete no longer bears tension, and most of the tensile force is then resisted by the steel bars. As loading continues to rise, damage at the upper edge of the bridge deck connection plate further develops. When the load reaches 1179.71 kN, the reinforcement at the modular expansion joints begins to yield, and the corresponding section moment is 959.67 kN·m. When the load increases to 1511.29 kN, the curve slope approaches zero, indicating that the connecting plate has reached its limit state in load-bearing capacity, and the section bending moment becomes 1091.58 kN·m.

Based on the above finite-element results, the load－displacement curve is obtained, as illustrated in Fig. 1. The curve shown in the figure can be divided into the following three stages:

(1) Elastic working stage. From the beginning of loading until cracking appears at the upper edge of the bridge deck connecting plate, the structure remains in the elastic stage, and the load－displacement curve is nearly a straight line. At this moment, the strain at the upper edge of the cross-section is 7.63×10^{-5}, and the corresponding cross-section bending moment is 112.53 kN • m.

(2) Elastic-plastic working stage. After cracks form at the upper edge of the bridge deck connecting plate and before the tensile reinforcement yields, the structure enters the elastic-plastic stage. Once cracking occurs at the upper edge of the plate, the tensile force is borne mainly by the steel reinforcement, while the concrete essentially ceases to sustain tensile stress. As the load continues to increase, the crack width enlarges and extends downward from the top. The tensile force of the structure was mainly borne by the steel reinforcement, and at this time, the concrete basically did not bear the tensile stress, and with the continuous increase of the load, the width of the crack increased, and expanded downward from the top plate of the connecting plate, and the nonlinear relationship of the connecting plate became more and more obvious. When the load increases to 1179.71KN, the reinforcement tensile stress exceeds the standard value of tensile strength, and the reinforcement at the bridge deck connecting plate starts to yield, and at this time the section moment is 959.67KN·m.

(3) Destruction stage. After the reinforcement yielding, as the load continues to increase, the assembled bridge also enters the yielding stage, as can be seen from the load-displacement curve, when it reaches the highest point, the assembled bridge basically reaches the limit state of the carrying capacity, at this time, the sectional bending moment is 1091.58KN·m, and at this time, the load is 1511.29KN.

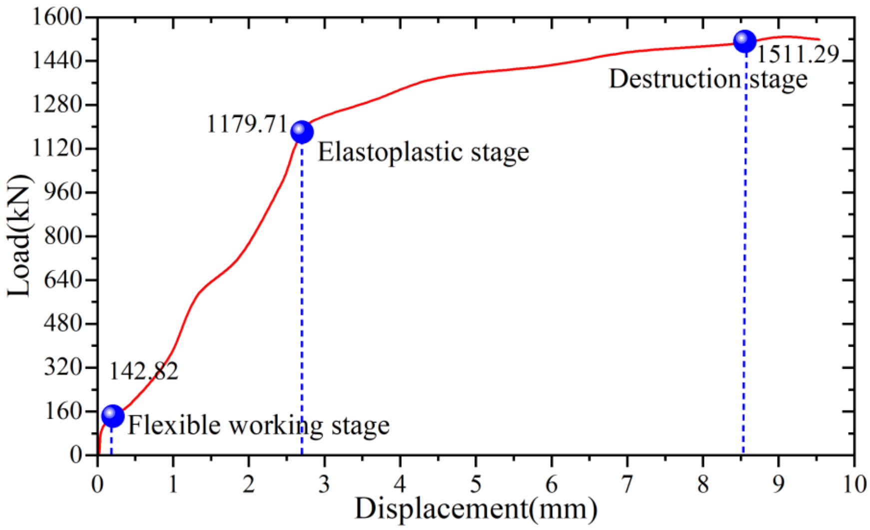

Figure 1: Load-displacement curve

4.1.2 Comparison of load capacity and deflection

In this research work, by the means of unidirectional cyclic loading test, comparisons have been made on the working characteristics of the bridge deck connecting plates in the assembled bridges under different reinforcing systems such as steel, BFRP, and GFRP, together with different reinforcement ratios of 1.5% and 0.75%. In this part, the simulation outcomes are compared with the experimental data so as to prove the correctness and validity of the established finite-element model. On this basis, further discussion will be made on the whole force-displacement response of the structure not easily seen in the structural experiments for future parametric studies.

On the basis of the maximum bearing capacity and mid-span deflection of the connection plate in the assembly of the bridge from finite element method analysis, the envelope curve of the load-deflection curve has been derived and the actual curve can be seen in Figure 2, in which (a)-(d) represent the finite element load-deflection curve of steel reinforcing, BFRP reinforcing, GFRP reinforcing (ratio of 1.5%), and GFRP reinforcing (ratio of 0.75%) respectively.

From the comparison above between the finite element load-deflection curve and the measured one, we know that the working characters of the connection plates under different reinforcement materials and different reinforcement ratios show common tendency qualitatively. When the deformation of the structure is small, the load required in the finite element to make the connection plate produce the same deflection as that of the structural test is slightly lower, and the load-deflection curves are fitted better. As the deflection increases, the loads obtained from the finite element calculations grow faster and start to be higher than the load values in the actual structure, with the maximum loads being 1.25 to 1.35 times the actual maximum loads. Under the same loading displacement, the maximum mid-span deflections of the connection plates obtained from the simulation are lower than the test values, and the errors of the calculation results of the maximum mid-span deflections of the FRP bar connection plates are within 6.5%, which is small, and the maximum error of the calculation results of the steel bar connection plates reaches about 10%.

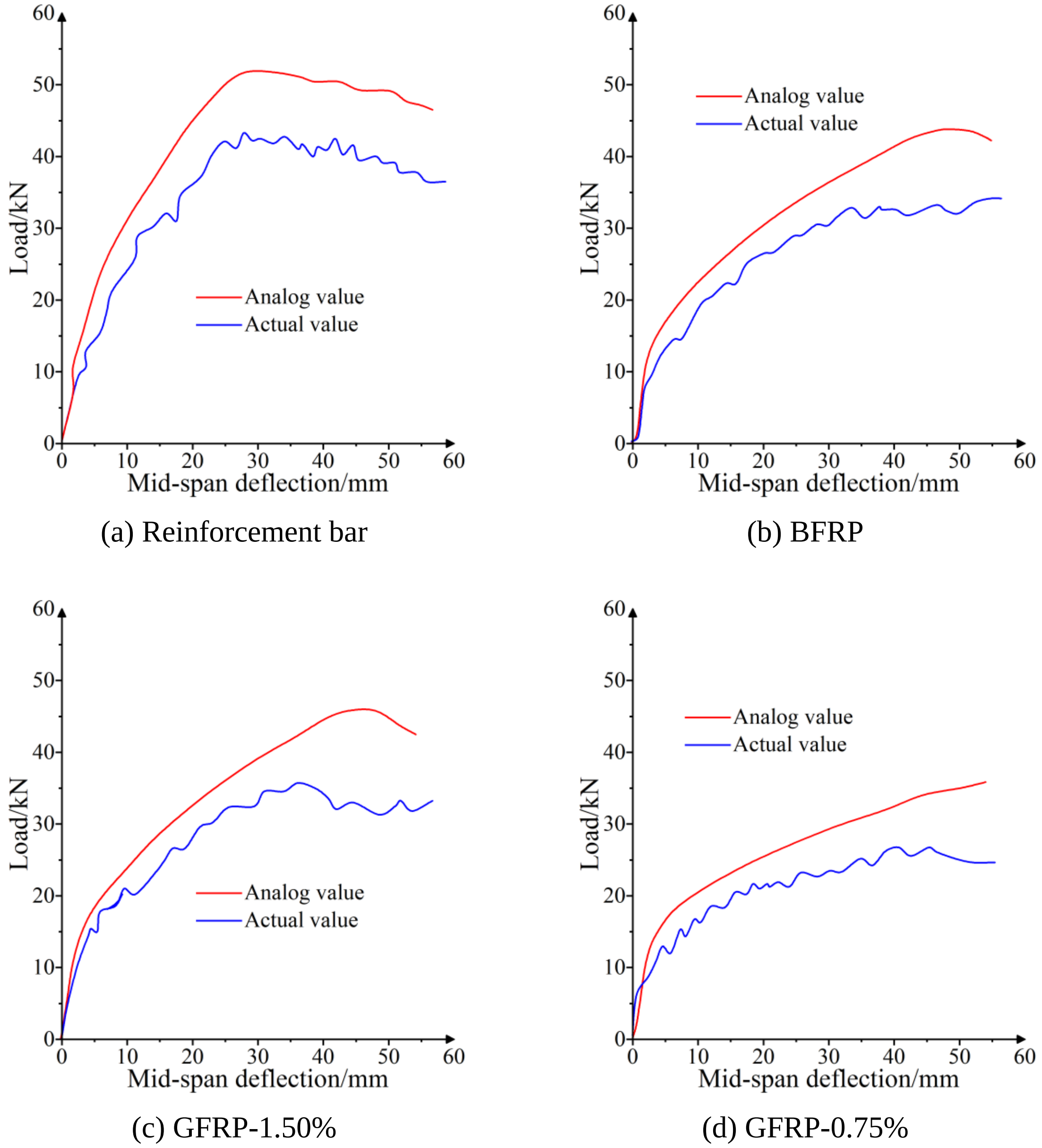

Figure 2: Comparison of load-mid-span deflection curves

The constitutive parameters of the material in finite-element simulation are obtained by matching the experimentally observed load-deflection curve to the theoretical one. As a result of the nonhomogeneity of the material and differences in test procedures, there occurs an inconsistency between the constitutive parameters and the real material parameters of the connecting plate. Thus, the initial stiffness of the connecting plate in the finite-element analysis turns out to be a little lower compared to that of the connecting plate, so the load corresponding to a certain deflection becomes a little lower than the real load. At the beginning of the testing procedure, cracks started to appear in the connecting plate, and then the load increasing rate decreased. During the test, the deformation pattern curve of the connection plate is more sharp due to the influence of crack development, which makes the mid-span deflection increase, while the material deformation of the connection plate in the finite element calculation is continuous and more uniform, and the deflection of the connection plate grows steadily with the increase of the deformation, which makes the calculated deflection smaller than the actual deflection.

For the reinforcing steel connection plate, with the increase of deformation in the test process, the connection plate reinforcement yielding, load-deflection curve on the envelope into the short platform section. The rapid increase in the deformation of the connection plate after the yielding of the reinforcement causes the material cracks to expand rapidly, the stiffness of the connection plate cross-section decreases rapidly, and then the load begins to decrease.

4.2 Fatigue deformation of assembled bridge expansion joints

4.2.1 Fatigue damage of expansion joints

The local analysis on the expansion-joint device model splits the externally applied load into the vertical component and the horizontal component. In this model, the definition of the horizontal component is in two directions: one is toward the expansion joint steel beam and defined as positive X-axis direction, while another is away from this expansion joint steel beam, called negative X-axis direction. Hence, there are two loading conditions in the expansion-joint device model; in which Condition 1 means loading in the positive X-axis direction and Condition 2 means loading in the negative X-axis direction.

When loading is applied by the wheel in this model, the movement of wheel is assumed to be in the positive X-axis direction; thus, the movement of wheel in negative X-axis direction is not included. This is because the two loading conditions give the same pattern of the stress history in terms of stress amplitude and peak stress. Since the fatigue damage estimation is based on the stress-amplitude or stress peak, then these parameters become the major concerns; not the evolution process of stress history.

The target of assembled bridge expansion joints should be the stability of the vehicle passing over them. From the finite-element modeling of assembled bridge expansion joints, the difference in the performance of assembled bridge expansion joints will be estimated depending on the material used. Figure 3 gives the variation graph of the principle stress when loading is being applied. Figure 4 shows the value of the maximum principal stress that appears at the location when the principle stress becomes maximum under the 120 kN loading case. Table 1 lists the critical-stress values for 120 kN wheel loading condition, and positive and negative stress values indicate the tension and compression stresses, respectively.

As shown in the table, in the conventional 120 kN axle load, the magnitude of the stress in any material is fairly low; even for the steel beam material with relatively higher compressive principal stress value, its maximum is about 4.5 MPa. It can be concluded from the transverse change of principal stresses in different materials that the transverse range of the single-wheeled load is mainly in the range of not more than 0.6m from the center line, and the principal stresses of all kinds of materials tend to be 0MPa by the time it is 0.9m, which means that in the single-wheeled load, the main stresses of the various materials tend to be 0MPa. That is to say, under the action of single wheel wheel load, in addition to the wheel contact range, the lateral influence of the extended range of not more than half of the lateral action distance of the wheel load, the vehicle maintains a safe distance from the lateral driving adjacent lanes of the vehicle wheel load action area does not overlap each other. This also shows to a certain extent that the overall fatigue damage change of the assembled bridge expansion joint is low, and it still maintains good stress reflection under the vehicle load.

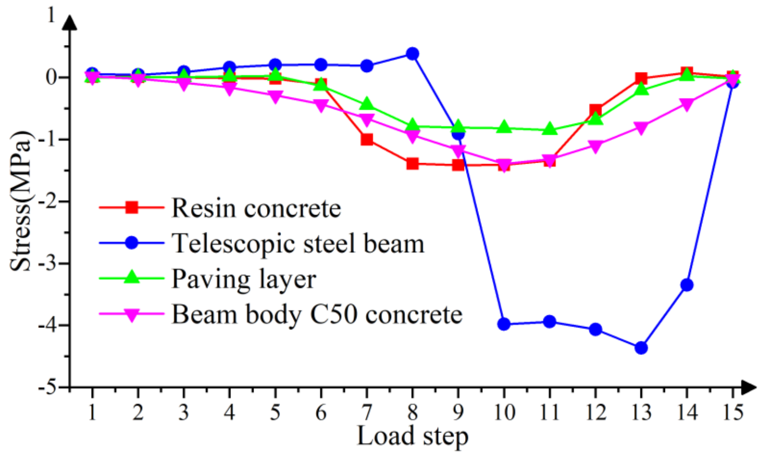

Figure 3: Principal stress of the main material

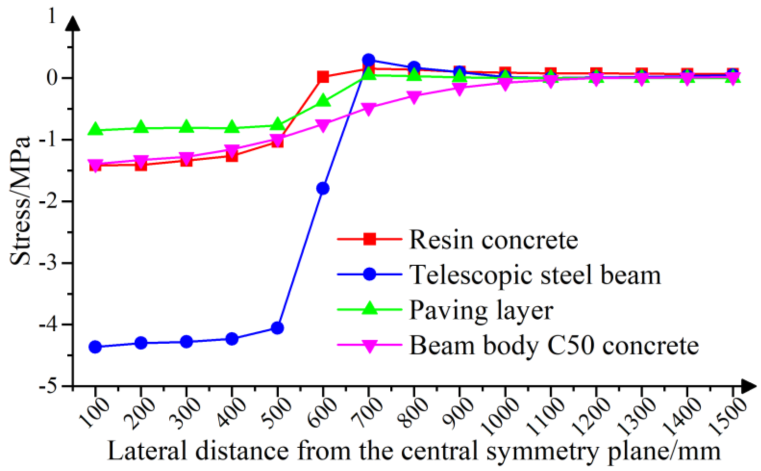

Figure 4: Lateral variation curve of principal stress

Table 1: Key stress values under a 120kN shaft load

Material	Max stress/MPa	Min stress/MPa	Stress amplitude/MPa
Resin concrete	-1.413	+0.074	1.487
Expansion joint steel beam	-4.364	+0.379	4.743
Asphalt pavement layer	-0.847	+0.027	0.874
Beam body C50 concrete	-1.396	+0.014	1.409

4.2.2 Trends in equivalent forces

The fatigue behavior study of assembled bridge expansion joints subjected to moving loads is extended here to see how the variation of the top plate, bottom plate, side plate, and rear plate thickness of bridge box can impact the force condition of assembled bridge expansion joints in assembled bridges. In this case, a standard static axle load of 120 kN has been used to analyze the situation by employing the finite element model discussed above in the previous part of this paper, and the equivalent stress field of assembled bridge expansion joints is presented in ANSYS.

In relation to the assembled bridge box, the top plate has a central position in the transverse direction, the bottom plate has a central position too in the transverse direction, and finally, the side plate is placed at the mid-position in the transverse direction. The measurement points of the holes in bottom and top plates are close to the 900 mm cross-section. Figure 5 shows the results of the simulation of stresses for different axle load situations.

By analyzing the simulated stress results at different locations of the assembled bridge under varying axle loads, the following conclusions can be obtained:

(1) The total length of the assembled bridge expansion joint is 4000 mm. Equivalent-stress response and strain deformation are both quite obvious at and near the loading surface, whereas the equivalent-stress response at the two ends of the joint and at mid-span is relatively small. This result is basically consistent with the conclusions derived from the actual static-load test data.

(2) The highest stress values in the bottom plate and the side plate of the box do not appear at the center of the loaded surface, but rather near the hole, indicating that structural changes around the hole affect the box force state to some extent. The peak stress in the side plate appears near the displacement box of the assembled bridge expansion joint.

(3) Because of the structural complexity of the assembled bridge expansion joint, strain gauges cannot be attached to the upper plate of the box to obtain the corresponding measured data. Therefore, the absence of test data can be supplemented through finite-element mechanical simulation.

(4) Under the same axle-load condition, the stress level of the upper plate and that around the hole of the upper plate at the same box cross-section is slightly greater than that of the bottom plate and the corresponding hole region. Compared with the simple steel box − concrete composite simply supported girder, the strain value of the bottom plate of the box is larger than that of the upper plate. This indicates that the assembled bridge expansion joint can effectively improve the bearing performance of the bottom plate under the support of a T-beam.

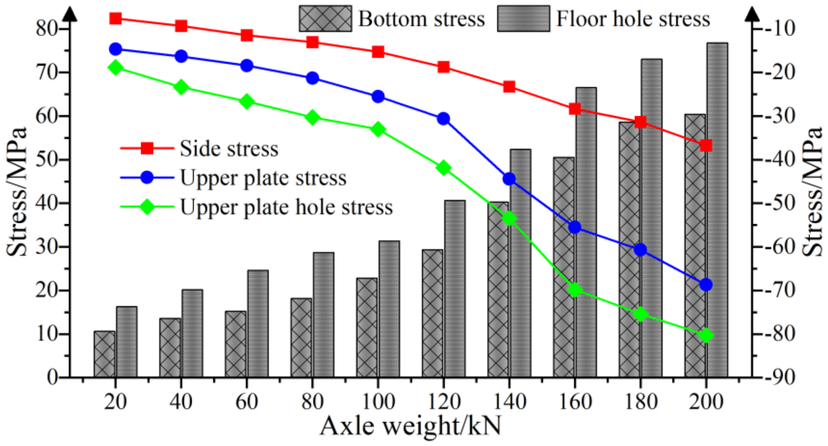

Figure 5: Simulation stress values of different measuring points in different axis

5 Conclusion

In the article, the damage and deformation mechanisms of expansion joints of assembled bridges were studied in terms of load-displacement, bearing capacity-deflection, fatigue damage, and the trend of change of equivalent stresses by using the ontological relationship and evolution equations of damage mechanics, and the finite element model was established by combining the finite element software, respectively. It was found that the cracking strain of concrete was 7.63×10^{-5}, the cracking moment of the cross-section of the deck connecting plate of the assembled bridge was 112.53KN·m. Changes in the bearing capacity and deflections are noted for bridges made from different types of materials. With the load on the axle being 120 kN, the stresses that act on each type of material are relatively small, with the maximum compressive stress never going beyond 4.5 MPa. Stresses that occur at different points in the expansion joint of the constructed bridge differ significantly. Destruction and deformation of the expansion joint can be prevented by using a T-beam.

Funding

Provincial Science and Technology Research and Development Program of Henan Province in 2025 Project: Research on the Failure Mechanism and Deformation Optimization Improvement Design of Expansion Joints in Prefabricated Highway Bridges (Project Number: 252102241016).

About the Author

Yujuan Liu was born in 1990 in Heze, Shandong. She received her master's degree from Shandong University of Science and Technology. She is currently teaching at the School of Intelligent Construction at Zhengzhou Business College, with her main research focus on building structure and bridge design, as well as performance analysis of building materials.

Chuan'ai Zhang was born in 1975 in Rizhao, Shandong. She obtained her doctoral degree from the PLA University of Science and Technology. Currently, she teaches at the School of Intelligent Construction at Zhengzhou University of Finance and Economics, with her main research focus on building structure design and performance analysis of building materials.

References

[1] Ni, Y. Q., Hua, X. G., Wong, K. Y., & Ko, J. M. (2007). Assessment of bridge expansion joints using long-term displacement and temperature measurement. Journal of Performance of Constructed Facilities, 21(2), 143-151.

[2] Wang, X., Zhao, P., & Tao, Y. (2018). Evaluating impacts of overloaded heavy vehicles on freeway traffic condition by a novel multi-class traffic flow model. Sustainability, 10(12), 4694.

[3] Lukoševičius, V., Makaras, R., Rutka, A., Keršys, R., Dargužis, A., & Skvireckas, R. (2021). Investigation of vehicle stability with consideration of suspension performance. Applied sciences, 11(20), 9778.

[4] Nie, J. G., Zhou, M., Wang, Y. H., Fan, J. S., & Tao, M. X. (2014). Cable anchorage system modeling methods for self-anchored suspension bridges with steel box girders. Journal of Bridge Engineering, 19(2), 172-185.

[5] Ding, Y., Zhang, W., & Au, F. T. (2016). Effect of dynamic impact at modular bridge expansion joints on bridge design. Engineering Structures, 127, 645-662.

[6] Lu, P., Wang, J., Ding, J., Wu, Y., Yang, L., & Gu, Z. (2025). Mechanical behaviour of bridge expansion joint interfaces filled with novel polyurethane-modified asphalt. Road Materials and Pavement Design, 26(5), 921-939.

[7] Hou, J., Wang, J., Xu, W., Chen, Y., Wang, B., Liu, J., ... & Sun, H. (2022). An analysis

method of vehicle–bridge coupling vibration considering effects of expansion joint parameters and its application. Structural Control and Health Monitoring, 29(11), e3065.

[8] Li, J., Li, P., Bi, Y., Chen, S., & Yang, C. (2025). Damage detection of modal bridge expansion joints using acoustic signal processing and SVDD. Measurement, 118963.

[9] Fu, C. C., & Zhang, N. (2011). Investigation of bridge expansion joint failure using field strain measurement. Journal of performance of constructed facilities, 25(4), 309-316.

[10] Gao, J., Zhang, X., & Lei, J. (2022). Evaluation of the Dynamic Impact of a Passing Vehicle on a Bridge Deck Due to a Damaged Expansion Joint. Symmetry, 14(4), 813.

[11] Deng, L., Yan, W., & Zhu, Q. (2016). Vehicle impact on the deck slab of concrete box-girder bridges due to damaged expansion joints. Journal of Bridge Engineering, 21(2), 06015006.

[12] Wedig, W. V. (2016). Jump phenomena in road-vehicle dynamics. International Journal of Dynamics and Control, 4(2), 213-220.

[13] Di Mascio, P., Loprencipe, G., Moretti, L., Puzzo, L., & Zoccali, P. (2017). Bridge expansion joint in road transition curve: Effects assessment on heavy vehicles. Applied Sciences, 7(6), 599.

[14] Abdel Raheem, S. E., & Hayashikawa, T. (2013, September). Mitigation measures for expansion joint effects on seismic performance of bridge structures. In Proceedings of the Thirteenth East Asia-Pacific Conference on Structural Engineering and Construction (EASEC-13) (pp. B-1). The Thirteenth East Asia-Pacific Conference on Structural Engineering and Construction (EASEC-13).

[15] Cho, H. M., Lee, H. W., Kim, K. S., & Park, K. T. (2024). Investigating the Application of Smart Materials for Enhanced Maintenance of Rubber Expansion Joints in Bridge Expansion Joint Systems. Applied Sciences, 14(7), 2828.

[16] Li, J., Wen, F., Chen, J., Yang, C., Du, W., Xu, L., & Li, P. (2023). Experimental study of bridge expansion joint damage based on natural frequency. Sensors, 23(14), 6437.

[17] Friedl, R., & Mangerig, I. (2017). Dynamic amplification of bridge-expansion-joints considering roughness induced vehicle vibrations. Procedia Engineering, 199, 2651-2656.

[18] Stamatopoulos, G. N. (2017). Fatigue life of the bolted yoke connection in single support beam (SSB) modular bridge expansion joints. International Journal of Steel Structures, 17(2), 723-738.

[19] Chang, L. M., & Lee, Y. J. (2002). Evaluation of performance of bridge deck expansion joints. Journal of performance of constructed facilities, 16(1), 3-9.

[20] Guo, T., Huang, L., Liu, J., & Zou, Y. (2018). Damage mechanism of control springs in modular expansion joints of long-span bridges. Journal of Bridge Engineering, 23(7), 04018038.

[21] Sun, Z., & Zhang, Y. (2016). Failure mechanism of expansion joints in a suspension

bridge. Journal of Bridge Engineering, 21(10), 05016005.

[22] Ma, Y., Peng, A., Wang, L., Zhang, C., Li, J., & Zhang, J. (2020). Fatigue performance of an innovative shallow-buried modular bridge expansion joint. Engineering Structures, 221, 111107.

[23] Ji, W., Shao, T., & Li, J. (2024). Analytical Investigation of Fatigue Behavior in a Modified Composite Steel Box Concrete Girder Bridge with Corrugated Steel Webs under Pavement and Expansion Joint Deterioration. Journal of Bridge Engineering, 29(10), 04024078.

[24] Sun, Z., & Ye, X. W. (2022). Incorporating site-specific weigh-in-motion data into fatigue life assessment of expansion joints under dynamic vehicle load. Engineering Structures, 255, 113941.

[25] Coelho, B. Z., Vervuurt, A. H. J. M., Peelen, W. H. A., & Leendertz, J. S. (2013). Dynamics of modular expansion joints: The martinus nijhoff bridge. Engineering Structures, 48, 144-154.

[26] Li, J., Wen, F., Pan, Y., Chen, J., & Yang, C. (2024). Experimental study on the damage identification of bridge expansion joints. Journal of Civil Structural Health Monitoring, 14(3), 575-590.

[27] Chen, Z. H., Liu, X. W., Zhou, G. D., Liu, H., & Fu, Y. X. (2021). Damage detection for expansion joints of a combined highway and railway bridge based on long-term monitoring data. Journal of Performance of Constructed Facilities, 35(4), 04021037.

[28] Ni, Y. Q., Wang, Y. W., & Zhang, C. (2020). A Bayesian approach for condition assessment and damage alarm of bridge expansion joints using long-term structural health monitoring data. Engineering Structures, 212, 110520.

[29] Dong, Y., Pan, Y., Wang, D., & Chen, A. (2024). Transformer-Enhanced Traffic Load Simulation for Wear Evaluation of Bridge Expansion Joint. Structural Control and Health Monitoring, 2024(1), 6631877.

[30] Ni, Y. Q., Hua, X. G., & Ko, J. M. (2006). Reliability-based assessment of bridges using long-term monitoring data. Key engineering materials, 321, 217-222.